HHS Public Access

Author manuscript

Science. Author manuscript; available in PMC 2023 May 15.

Published in final edited form as:

Science. 2023 April 21; 380(6642): eabn7625. doi:10.1126/science.abn7625.

Oncogenic *CDK13* Mutations Impede Nuclear RNA Surveillance

Megan L. Insco[1,2,*], **Brian J. Abraham**[3], **Sara J. Dubbury**[4,5], **Ines H. Kaltheuner**[6], **Sofia Dust**[6], **Constance Wu**[1], **Kevin Y. Chen**[1], **David Liu**[2], **Stanislav Bellaousov**[7], **Anna M. Cox**[1], **Benjamin J.E. Martin**[8], **Tongwu Zhang**[9], **Calvin G. Ludwig**[1], **Tania Fabo**[1], **Rodsy Modhurima**[1], **Dakarai E. Esgdaille**[7], **Telmo Henriques**[8], **Kevin M. Brown**[9], **Stephen J. Chanock**[9], **Matthias Geyer**[6], **Karen Adelman**[8], **Phillip A. Sharp**[4,5], **Richard A. Young**[5,10], **Paul L. Boutz**[7,11,12], **Leonard I. Zon**[1,*]

[1]Stem Cell Program and Division of Hematology/Oncology, Boston Children's Hospital, Howard Hughes Medical Institute, Boston, MA, 02115, USA.

[2]Department of Medical Oncology, Dana-Farber Cancer Institute, Boston, MA, 02115, USA.

[3]Department of Computational Biology, St. Jude Children's Research Hospital, Memphis, TN, 38105, USA.

[4]The David H. Koch Institute for Integrative Cancer Research, Massachusetts Institute of Technology, Cambridge, MA, 02139, USA.

[5]Department of Biology, Massachusetts Institute of Technology, Cambridge, MA, 02139, USA.

[6]Institute of Structural Biology, University of Bonn, Bonn, 53127, Germany.

[7]University of Rochester School of Medicine and Dentistry, Rochester, NY, 14642, USA.

[8]Department of Biological Chemistry and Molecular Pharmacology, Harvard Medical School, Boston, MA, 02115, USA.

[9]Division of Cancer Epidemiology and Genetics, National Cancer Institute, Rockville, MD, 20850, USA

[10]Whitehead Institute for Biomedical Research, Massachusetts Institute of Technology, Cambridge, MA, 02142, USA.

[11]Center for RNA Biology, University of Rochester, Rochester, NY, 14642, USA.

[12]Center for Biomedical Informatics, University of Rochester, Rochester, NY, 14642, USA.

[*]Corresponding authors: leonard.zon@enders.tch.harvard.edu and Megan_Insco@dfci.harvard.edu.

Author contributions. M.L.I. planned and performed the experiments with assistance from K.Y.C., T.F., A.M.C., R.M., and C.W. with the following exceptions. Mouse ES cell experiments were planned/performed by S.J.D. and kinase assays were planned/performed by I.H.K and S.D. Data were analyzed by M.L.I., B.J.A., P.L.B., S.B., B.E.J.M., C.G.L., T.Z, and D.E.E. D.L. coded the survival analysis. M.G. provided the plots of the mutations on the CDK13 crystal structure and insight into the effects the mutations could have on CDK13 function. T.H. advised on TT-seq experiments. R.A.Y., P.A.S., P.L.B., K.A., M.G., K.M.B, S.J.C, and L.I.Z. supervised the project. M.L.I, B.J.A., P.L.B., and L.I.Z. wrote the manuscript.

Competing Interests. R.A.Y. is a founder and shareholder of Syros Pharmaceuticals, CAMP4 Therapeutics, Omega Therapeutics, and Dewpoint Therapeutics. P.A.S. is a shareholder of Syros Pharmaceuticals. L.I.Z. is a founder and stockholder of Fate Therapeutics, CAMP4 Therapeutics, and Scholar Rock. He is a consultant for Celularity. B.J.A. is a shareholder in Syros Pharmaceuticals. K.A. consults for Syros Pharmaceuticals and is on the scientific advisory board of CAMP4 Therapeutics. P.L.B. is a paid scientific consultant for Skyhawk Therapeutics, Inc. All other authors declare that they have no competing interests.

Abstract

RNA surveillance pathways detect and degrade defective transcripts to ensure RNA fidelity. We find disrupted nuclear RNA surveillance is oncogenic. Cyclin Dependent Kinase 13 (*CDK13)* is mutated in melanoma and patient-mutated *CDK13* accelerates zebrafish melanoma. *CDK13* mutation causes aberrant RNA stabilization. CDK13 is required for ZC3H14 phosphorylation, which is necessary and sufficient to promote nuclear RNA degradation. Mutant CDK13 fails to activate nuclear RNA surveillance, causing aberrant protein-coding transcripts to be stabilized and translated. Forced aberrant RNA expression accelerates melanoma in zebrafish. We find recurrent mutations in genes encoding nuclear RNA surveillance components in many malignancies, establishing nuclear RNA surveillance as a tumor-suppressive pathway. Activating nuclear RNA surveillance is crucial to avoid accumulation of aberrant RNAs and their ensuing consequences in development and disease.

Transcriptional Cyclin Dependent Kinases (CDKs) are a family of kinases activated by a cyclin binding partner (1, 2) that have roles in controlling transcriptional subprocesses including initiation, elongation, co-transcriptional RNA processing, and termination (3–9). Transcriptional CDKs, including CDK13, are being investigated as therapeutic targets for many difficult-to-treat cancers (10–14). Mutations affecting CDK13 cause syndromic developmental disorders that affect neural crest-derived tissues (congenital heart defects, dysmorphic facial features, and intellectual development) (15–19). The role of CDK13 in transcription and RNA processing remains poorly understood.

RNA polymerase II (RNAPII) is exquisitely regulated to ensure that transcriptional initiation, elongation, co-transcriptional processing, and termination are precisely executed on protein-coding genes. During elongation, a rapid cascade of RNA processing steps takes place (20). RNA processing errors can result in aberrant transcripts that must be degraded by RNA surveillance pathways. Messages that prematurely terminate are predicted to evade nonsense mediated decay (NMD) due to lack of downstream splice events (21) and require a complementary surveillance pathway to avoid accumulation and translation of pathogenic transcripts.

Aberrant or unstable nuclear RNAs are recognized by adaptor complexes, which recruit the MTR4 helicase and the nuclear RNA exosome degradation complex to specific RNAs. The recently reported PolyA eXosome Targeting (PAXT) complex targets prematurely terminated RNAs (ptRNAs) for degradation (22, 23). How ptRNAs (and not messenger RNAs [mRNAs]) are specifically targeted for PAXT degradation is unknown.

In this study, we find that patient-specific mutations in CDK13 accelerate oncogenesis in human cells and a zebrafish melanoma model and that CDK13 is responsible for activating nuclear RNA surveillance. When CDK13 is mutated or lost, phosphorylation of the PAXT component, ZC3H14, is compromised, and ptRNAs fail to be targeted for nuclear degradation. Consequently, stabilized ptRNAs are translated into truncated proteins. Overexpression of ptRNAs leads to accelerated melanoma in zebrafish. We find that PAXT subunits recruited by CDK13 phosphorylation are mutated in 17% of melanomas and that recurrent mutations in PAXT subunits ZFC3H1 and ZC3H18 occur in many cancer

types. This work demonstrates that CDK13 normally activates nuclear RNA surveillance machinery to degrade oncogenic prematurely terminated RNAs.

Results

CDK13 has properties consistent with a tumor suppressor.

We initially examined the transcriptional CDK loci as defined by (2) in melanoma patient samples from The Cancer Genome Atlas (24) and found CDK13 was mutated in 4.6% of patients and had a cluster of mutations near the ATP-binding site (Table S1). We then analyzed a larger set of publicly available patient data (24–33) specifically for CDK13 mutations and found *CDK13* is somatically mutated in 3.9% of cutaneous melanomas (52/1347 patients) (Figure S1A, Table S2). To determine if *CDK13* somatic mutations are selected for in melanoma, OncodriveFM (34) was used because it accounts for background mutational load and predicted mutational severity. This analysis suggested that *CDK13* is a FDR-significant melanoma driver gene (q=0.042, p=0.0049). We observed 2.2-fold enrichment of deleterious mutations in the kinase domain vs. the remainder of the protein (Fisher's exact test, p = 0.03, OR = 5.4) (Figure 1A red and orange, Figure S1A, Table S2, Data S1). To assess *CDK13* mutational clonality, we identified samples that were copy-neutral for *CDK13* and compared the variant allelic fraction (VAF) of *CDK13* mutations to known driver mutations from the same samples (24). Of six evaluable tumors, four were clonal (P746T, R860Q, E1248K, and P881L), one was subclonal (R1206M), and one was potentially subclonal (E1448X) with a VAF similar to *NF1* (Figure S1B, Data S1). In non-copy-neutral *CDK13* mutant samples, we observed additional samples harboring clonal or potentially clonal *CDK13* mutations (9/12). Of the 7 samples with clonal *CDK13* mutations, all were heterozygous. *CDK13* is mutated in many other malignancies (Figure S1C), which also display an enrichment in kinase domain mutations (1.8x, n=13269 from 56 studies, $p=2.47\times10^{-13}$) (Data S1). Loss of heterozygosity is infrequently observed in melanoma. Of the 1347 melanoma patient samples, we assessed those with copy-number and mutational information for loss of heterozygosity and identified that 0.5% had biallelic loss (n=832, one biallelic deletion and three with a mutation and heterozygous deletion). These data show that *CDK13* is a mutated driver gene with a modest enrichment in kinase domain mutations, suggesting that kinase domain mutations have additional selection pressure beyond loss of function, such as dominant negative activity.

De novo heterozygous CDK13 kinase-domain mutation has been reported to cause a CDK13-associated developmental syndrome (80%, 32/40 patients) (15–19), suggesting functional importance of these mutations. All but two of the CDK13-developmental kinase domain variants are found as somatic mutations in cancer. The notable difference is the N842 variant, the most common variant associated with the developmental disorder, which was not found as a somatic mutation in melanoma or non-melanoma cancer (Data S1). While *CDK13* was not considered a driver gene in prior studies due to its low mutational rate, these data show that *CDK13* is a broadly-utilized driver gene with an enrichment in deleterious kinase-domain mutations, suggesting a function beyond haploinsufficiency.

If mutant CDK13 functions by interfering with WT CDK13, in other words has dominant negative activity, then mutant CDK13 would be expected to result in a similar phenotype

to *CDK13* downregulation. Survival analysis using human TCGA melanoma patient (24) data revealed that patients with *CDK13* downregulation (z score ≤ −1.0, fold change 0.48) or somatic mutation (*CDK13*-altered) combined had decreased overall survival (Figure 1B, S1D–E, log rank p = 0.0028). *CDK13* alteration remained associated with poor survival after adjustment in a multivariate model (HRR = 1.81 [95% CI [1.13–2.90], Cox p = 0.014, Table S3). Patients initially staged with 0/1/2 melanoma that had *CDK13*-alterations exhibited reduced overall survival compared to remaining stage 0/1/2 melanoma patients (Figure S1F, log-rank p = 0.0012). The percentages of *CDK13*-altered (mutated or downregulated) melanomas with $BRAF^{V600}$ mutations or $NRAS^{Q61}$ were compared to the remaining cases in the TCGA melanoma cohort (24), and no significant differences were found (chi squared test, p=0.287) (Table 1). These data suggest *CDK13* mutation or downregulation are associated with poor overall survival in melanoma patients.

CDK13 melanoma mutations that occur in the kinase domain were projected onto a previously solved crystal structure (Figure 1C) (35). The P869 residue is located two residues away from the T871 phosphorylation site and the R860 residue normally coordinates with phospho-T871, so these mutations could disrupt kinase activation. The W878 mutation may change the substrate binding pocket and mutants P881L, P893L, and I843N might disrupt the integrity of the kinase domain structure. In vitro, $CDK13^{WT}$ activated by its canonical cyclin partner, Cyclin K (CCNK), had robust kinase activity while the R860Q, W878L, and K734R mutants failed to phosphorylate full-length RNAPII C-terminal domain (CTD_{52}) and a second substrate (Figure 1D, S1G), but maintained Cyclin binding (Figure S1G, right). The $CDK13^{K734R}$ mutation replaces the lysine required for catalysis (36) and occurs in the CDK13-associated developmental syndrome (15). These data show that CDK13 mutations observed in melanoma abrogate kinase activity.

To examine the role of CDK13 in melanoma, the MAZERATI rapid modeling system was used with *mitfa:*$BRAF^{V600E}$*; p53−/−; mitfa−/−* zebrafish, hereafter referred to as the “Triples” zebrafish melanoma model. These zebrafish lack Mitfa, the master regulator of melanocyte development, and lack melanocytes (37–39). Melanocytes were rescued with a vector that expresses Mitfa, allowing cell-autonomous melanocyte-specific gene expression or CRISPR/Cas9-mediated inactivation using the *mitfa* promoter. Zebrafish with melanocyte-specific CRISPR-deletion of zebrafish *cdk13* as compared to that of a control gene showed significantly decreased melanocyte numbers (one-way ANOVA q=0.0030), indicating that *cdk13* is required for melanocyte development (Figure 1E–F, S1H–I). Overexpression of human wild-type CDK13 ($CDK13^{WT}$) also resulted in fewer melanocytes during development (Figure 1E–F, S1J) but was able to rescue melanocyte number loss caused by *cdk13* deletion (Figure 1E–F, S1K). Rarely, melanomas arose in zebrafish with *cdk13* melanocyte-specific CRISPR-deletion, and phospho-histone 3 (PH3) immunohistochemical (IHC) staining revealed that *cdk13* CRISPR-deleted vs. control melanomas were significantly more proliferative (Mann-Whitney two-tailed t test, p = 0.014) (Figure 1G, S1L–M). Proper Cdk13 levels are required for melanocyte development and human CDK13 complements the loss of zebrafish *cdk13.*

To test whether CDK13 melanoma patient mutations cause more aggressive melanoma *in vivo*, mutant CDK13 was expressed in melanocytes in the Triples zebrafish melanoma

model. Control enhanced green fluorescent protein (*EGFP)* expression resulted in expected rescue of mosaic stripes; whereas human CDK13^{WT} expression resulted in few melanocytes at 9 weeks-post-fertilization (wpf), so CDK13^{WT}-expressing animals were not followed for tumor onset. In contrast, overexpression of CDK13^{R860Q}, CDK13^{P869S}, CDK13^{W878L}, CDK13^{P881L}, or CDK13^{P893L} caused the appearance of black patches at 9 wpf (Figure 1H, S1N) and expedited tumor onset (Figure 1I, S1O–P). Because all tested *CDK13* mutations promoted melanoma to a similar degree, we have used them interchangeably in most assays (hereafter called *CDK13^{mut}*). CDK13^{mut}-expressing melanomas had more PH3-positive cells by IHC than controls (Figure 1J, S1Q). Since both melanocyte-specific *cdk13* CRISPR-deletion and forced human CDK13^{mut} expression caused more proliferative melanomas, our data support that CDK13^{mut} acts through a dominant negative or antimorphic mechanism, wherein human CDK13^{mut} adversely affects intact zebrafish Cdk13^{WT} activity. Our data are consistent with the existing human developmental disorder genetics showing that CDK13 mutations work via a dominant negative mechanism (15–19).

We hypothesized that Cyclin-binding is required for CDK13^{mut} dominant negative activity. To test whether CCNK (35, 40–42) or Cyclin T1 (CCNT1) are required for CDK13^{mut} dominant negative melanomagenesis *in vivo*, we co-injected vectors that express melanocyte-specific CDK13^{mut} and that delete *ccnK* or *ccnT1* in the Triples zebrafish melanoma model. *ccnK* melanocyte-specific inactivation expedited melanoma in the presence of CDK13^{W878L}, but not alone (Figure S1R–S). *ccnT1* melanocyte-specific inactivation suppressed CDK13^{W878L} and CDK13^{R860Q} oncogenesis but had no effect alone (Figure 1K–L, S1T–U). These data indicate that the oncogenic mechanism of CDK13^{mut} requires CCNT1.

To determine the effect of mutant CDK13 expression in human melanoma cells, CLOVER fluorescent protein, CDK13^{WT}, CDK13^{W878L}, or CDK13^{R860Q} was expressed in human A375 melanoma cells. Cells expressing either CDK13 mutant had a decreased doubling time (increased growth rate) compared to CDK13^{WT} or CLOVER (Figure 1M, Figure S1V). These data show that mutant CDK13 expression causes human melanoma cells to proliferate more quickly, indicating that mutant CDK13's pro-proliferative function is conserved.

CDK13 mutation results in accumulation of RNAs that prematurely terminate in introns.

As CDK13 is phylogenetically related to known transcriptional kinases, we tested for a global RNA phenotype by quantifying differential exon usage. Differential expression analysis of first (F), alternative first (AF), internal (I), last (L), or alternative last (AL) exons in each gene was performed in zebrafish melanomas. We observed significantly increased read coverage in the first exon as compared to the last exon in CDK13^{mut}-expressing vs. control melanomas (two-sided Wilcoxon rank sum test $p<2.2\times10^{-16}$) (Figure 2A, S2A). These data suggest that prematurely terminated RNAs (ptRNAs) are present in CDK13^{mut} zebrafish melanomas.

Analysis of poly-A-selected RNA-sequencing (RNA-seq) from patient melanomas (patient characteristics in Table S4 showed that patients with CDK13^{mut}-expression vs. CDK13^{WT}-expression had increased read coverage in the first exon vs. the last exon (Figure 2B), indicating presence of ptRNAs. ptRNA evidence was of greater magnitude in the patient

RNA-seq data that were poly-A-selected as compared to non polyA selected, indicating that ptRNAs are polyadenylated (Figure 2B vs. 2A). We generated mouse embryonic stem cells (mESCs) that were *Cdk13*−/− and carried a doxycycline-inducible mouse *Cdk13* rescue transgene. Poly-A-selected RNA-seq was done at time zero (CDK13-expressed) and at 48 and 72 hours after doxycycline removal (CDK13-depleted) (Figure S2B–D). mESCs that were CDK13-depleted for 48 hours showed evidence of accumulated ptRNAs, with this effect intensifying at 72 hours post-depletion (Figure 2C). Accumulated ptRNAs in CDK13-depleted mESCs were largely non-overlapping from CDK12-depleted mESCs generated analogously (7) (Figure S2E, Data S1). These data show that CDK13's role in preventing accumulation of polyadenylated ptRNAs is conserved.

To determine where ptRNAs terminate in CDK13^{mut} melanomas, 3' RNA-seq was pursued. 3' sequencing was executed on Triples zebrafish melanomas with melanocyte-specific expression of EGFP (n=3) or mutant CDK13^{mut} (n=3) and human melanoma A375 cells expressing CLOVER (n=2) or CDK13^{mut} (n=2). 83,660 overall recurrent termination events were identified in zebrafish melanomas and 47,787 overall termination events were identified in human melanoma cells. We used DEXSeq (43) to quantify differential usage of polyA termination sites between CDK13^{mut} and eGFP condition in zebrafish melanomas, which identified 802 significantly different termination events ($q< 0.05$). Parallel analysis from human melanoma cells revealed 1678 significantly different termination events ($q<0.05$) in CDK13^{mut} compared to control CLOVER cells. To determine whether conserved genes or pathways were affected in zebrafish and human melanomas, affected zebrafish genes were transferred to the nearest ortholog and the gene lists were overlapped. Only 3.4% of genes were found in both lists and gene ontology analysis showed no enriched pathways using the "biologic process complete" annotation set. Given the lack of shared functional pathways, these data suggest that the proliferative phenotype observed in CDK13 mutant patient melanomas, zebrafish melanomas, and human melanoma cells may be promoted by cellular stress from accumulated truncated RNAs, as opposed to truncation of a specific conserved target gene(s).

A significant increase in intronic cleavage sites was observed in CDK13^{mut} zebrafish melanomas (Figure 2D) and human melanoma cells (Figure 2E). In zebrafish melanomas, the significantly changed sites were enriched in introns (2.54 median fold change) and depleted from untranslated regions (UTRs) (−1.51 median fold change) ($p < 2.2 \times 10^{-16}$, two-sided Kolmogorov-Smirnov test); and in human melanoma cells the significantly changed sites were also enriched in introns (0.38 median fold change) and depleted from UTRs (−1.67 median fold change) ($p = 9.99 \times 10^{-16}$, two-sided Kolmogorov-Smirnov test). In CDK13^{mut} human melanoma cells, *SUV39H1* and *CBFB* each showed an upregulated ptRNA that terminated in the third intron (Figure 2F; S2F), while *TP53* had an upregulated ptRNA that terminated in the first intron (Figure S2G). For many upregulated intronic polyadenylation sites, a canonical RNA polyadenylation site (PAS) motif was observed (Figure 2F, S2F–G). These data show that CDK13^{mut} causes accumulation of ptRNAs generated from existing cleavage and polyadenylation sites found in intronic DNA in zebrafish and humans.

ptRNAs could accumulate from increased production or decreased clearance in CDK13 mutant cells. If transcription elongation is impaired, then ptRNAs should be produced at a higher rate at the expense of full-length mRNA synthesis. In this case, the absolute amount of first exon expression in CDK13 mutant cells should be unchanged compared to control; whereas the last exon expression should be decreased (Model 1, Figure 2G). Alternatively, if ptRNA clearance is decreased in CDK13^{mut} cells, then ptRNA concentration should rise without affecting full-length mRNA expression. The first exon expression should increase, while the last exon expression should remain stable (Model 2, Figure 2G). We hypothesized that absolute quantification of RNA species could help distinguish between these two models.

To measure concentration of ptRNAs and full-length mRNAs, digital droplet PCR (ddPCR) was performed for 4 genes with upregulated ptRNAs and two control genes, which were identified from the 3' sequencing described above. Signal from first exon probes represented both ptRNAs and full-length mRNAs while signal from last exon probes represented full-length mRNAs alone (Figure 2H, S2H). Fold change between CDK13^{mut} and control cells showed that all genes with predicted ptRNAs had an increase in first exon expression, consistent with ptRNA accumulation in CDK13^{mut} cells (*CBFB, LATS2, SUV39H1, TP53*). Neither control gene showed evidence of accumulated ptRNAs (*C1orf35, AGPAT1*). All 6 genes showed unchanged last exon expression in CDK13^{mut} cells as compared to control cells (Figure 2H). These data verify increased ptRNA levels in human CDK13^{mut} human melanoma cells. Last exon expression was intact for all genes tested, showing that transcription is intact and suggesting that ptRNAs accumulate in CDK13^{mut} cells via lack of clearance (Figure 2G, Model 2).

Prematurely terminated RNAs accumulate post-transcriptionally and are translated - including intronic sequences.

To directly examine transcription in CDK13^{mut}-expressing human melanoma cells, genome-wide nascent RNA production was measured via transient transcriptome sequencing (TT-seq) alongside paired standard RNA-seq (TT-seq schematic, Figure 3A) (44). If ptRNAs are generated through impaired transcriptional elongation, there should be less 4-thiouridine (4sU) incorporation at the 3' ends of genes (Figure 3A, Model 1). If ptRNAs accumulate via a post-transcriptional process such as impaired degradation, 4sU incorporation should be intact at the 3' ends of genes (Figure 3A, Model 2). RNA-seq differential exon analysis confirmed increased 5' coverage in CDK13^{mut} cells consistent with accumulated ptRNAs (Figure S3A). TT-seq metagenes showed no evidence of an increase in premature termination by RNAPII; instead, we observed a slight increase in RNA synthesis across the gene body in CDK13^{mut} cells (Figure 3B). In both TT-seq and RNA-seq, the metagene profiles indicate intact cleavage and polyadenylation in CDK13^{mut} and CLOVER control cells (Figure S3B–C). Nascent RNA production upstream of the cleavage and polyadenylation site is intact in CDK13^{mut}-expressing human melanoma cells further showing that elongation is functional (Figure S3B). These data show that CDK13^{mut} cells maintain productive RNAPII elongation. ptRNAs accumulate via a post-transcriptional mechanism such as loss of ptRNA degradation.

To measure production and steady-state levels of ptRNAs at intronic polyadenylation (IPA) sites in CDK13^{mut} cells, TT-seq and RNA-seq read coverage were quantified across IPA sites regulated by CDK13 as measured from 3' seq from Figure 2E ($q<0.1$). To allow pure intronic read quantification, IPA sites were included if they were >400bp from the nearest exon (n=134). The upstream/downstream coverage ratio for IPA sites from CDK13^{mut} vs. control human melanoma cells was compared to the median ratio in the RNA-seq and the TT-seq (Figure 3C). The upstream/downstream coverage ratio in the TT-seq (nascent RNA) was unaffected in CDK13^{mut} cells (Figure 3D, TT-seq, left), showing that there is similar low-level intronic transcriptional termination. In contrast, the RNA-seq upstream/downstream coverage ratio was significantly increased in CDK13^{mut} cells ($p=0.01$) (Figure 3D, RNA-seq, right; Figure S3D–E), reflecting higher steady-state RNA levels upstream of IPA sites. These data show that CDK13^{mut} cells stabilize ptRNAs post-transcriptionally.

To further investigate the transcriptional effects of chronic CDK13^{mut} expression, we performed Chromatin IP sequencing with antibodies to RNAPII (8WG hypophosphorylated and Ser2 CTD) in CDK13^{mut} and control human melanoma cells and zebrafish melanomas. In both systems, increased RNAPII occupancy was observed in gene bodies in the CDK13^{mut} condition (Figure S3F–J). These data support the ddPCR and TT-seq results showing that transcriptional elongation is intact and that ptRNA accumulation occurs in CDK13^{mut} via a highly conserved post-transcriptional mechanism.

ptRNAs have been reported to be exported (23, 45) and are predicted to be translated (21). We used tandem mass spectrometry to analyze global protein expression in melanomas isolated from age-matched Triples zebrafish with melanocyte-specific expression of CDK13^{mut} (n=3) or EGFP (n=3). Differential protein expression analysis revealed 174 proteins were upregulated, including 32 proteins related to vesicle-mediated transport with many implicated in lysosomes/autophagy (biologic complete, q = 2.3 e-13) (Figure S3K). CDK13^{mut} melanomas have increased lysosomal and autophagic protein expression, suggesting CDK13^{mut} cells have proteomic stress that could be caused by translation of truncated RNAs into truncated proteins.

If ptRNAs are translated, then there should be increased peptide levels at the beginning of proteins and fewer at the end of proteins (Figure 3E). To test whether ptRNAs are translated, individual peptide measurements filtered for changed between CDK13^{mut} and control conditions were analyzed ($p<0.1$). Log2 fold change CDK13^{mut} vs. EGFP control peptide measurements were binned and plotted as a percentage of canonical protein sequence length. This analysis revealed that early (N-terminal) protein peptide measurements were increased in CDK13^{mut} melanomas (Figure 3F). The negative slope is consistent with an increase in short proteins arising from the translation of prematurely terminated transcripts, analogous to increased 5' coverage in RNA-seq seen in CDK13^{mut} melanomas. This analysis identified 263 proteins with evidence of truncation. Any protein with >3 peptide measurements was tested for evidence of truncation which identified 103 truncated proteins, including 56 newly identified proteins (Figure S3L). Several identified truncated proteins are predicted to lose carboxy-terminal enzymatic domains, including Ilk, Crk, Ikbkb. The melanoma tumor suppressor Idh2 was also affected (Figure 3G, S3M) (46–48). These data show that, rather

than being degraded by the nuclear exosome, ptRNAs are being exported and translated into truncated proteins in CDK13^{mut}-expressing cells.

We asked whether intronic sequences at the end of ptRNAs are translated (schematized in Figure 3E). ptRNA translation products were predicted by assuming in-frame translation from the upstream exon until the first stop codon prior to ptRNA termination as determined from 3' seq. ptRNA translation products were added to the canonical proteome for tandem mass spectrometry data search. As predicted, intronic peptides were enriched specifically in the CDK13^{mut} zebrafish melanomas (Figure 3H). The abundance of some intronic peptides approached that of medium- to lowly-expressed full-length proteins (Figure S3N–P). To verify truncated protein expression, we selected two predicted truncated proteins with available N-terminal antibodies for immunoblotting. We identified truncated protein products from CRBN and CDK13 itself from CDK13-mutant expressing vs. control human melanoma cells (Figure S3Q–R). These data indicate that some ptRNAs from the CDK13 mutant melanomas are translated, including the intronic sequence preceding IPA sites, which could result in production of tumor-specific neoantigens.

Mutant CDK13 disrupts the polyA RNA exosome.

To elucidate how CDK13^{mut} expression results in ptRNA accumulation via a post-transcriptional mechanism, CDK13^{WT} was tagged, transiently expressed, and immunoprecipitated (IPed) from human melanoma cell nuclear extracts and co-IPed proteins were identified by mass spectrometry (MS) (Figure 4A). CDK13^{WT} IP-MS identified 37 proteins enriched in the CDK13^{WT} IP vs. control (Figure 4B). The most enriched ontology among these 37 proteins was "mRNA 3' end processing" (Reactome, FDR = 7.15 e-13) (49). CDK13 bound CCNT1 (Figure 4B–C), again implicating CCNT1 as an important binding partner for CDK13 in melanoma as our functional data suggested (Figure 1K–L; Figure S1U). The canonical cyclin-binding partner of CDK13, CCNK, was detected at levels above background but below thresholding. No other Cyclins were detected above background. Native CDK13 IP identified CCNT1 and CCNK by immunoblot (Figure S4A). This unbiased approach suggests that CDK13 binds CCNT1 in addition to CCNK in melanoma.

Of the enriched proteins in the CDK13^{WT} IP (Figure 4C), both PABPN1 and ZC3H14 interact with the PolyA tail eXosome Targeting (PAXT) complex (22), which is responsible for targeting ptRNAs for degradation (23). CDK13 binding to ZC3H14 was verified by immunoblot (Figure S4B. As ptRNAs accumulate in CDK13^{mut} melanoma via a post-transcriptional mechanism, and ptRNAs are degraded by the PAXT complex (50), we hypothesized that CDK13 normally works to activate PAXT. We hypothesized that loss of CDK13 kinase activity would fail to activate PAXT, leading to accumulated ptRNAs in melanoma.

As PABPN1 and ZC3H14 are genetically antagonistic (51, 52) and because we observed more ZC3H14 in our CDK13^{WT} IP, we chose to characterize ZC3H14 phosphorylation and binding partners in the presence and absence of CDK13 kinase activity. The nuclear isoform of ZC3H14 and a control protein were tagged, transiently expressed, and IPed from CDK13^{WT} and CDK13^{mut} human melanoma cells (Figure S4C; white, black, and blue).

IPed ZC3H14 from CDK13^{WT} cells had four phosphorylation sites, while in CDK13^{mut} cells, ZC3H14 lost phosphorylation only at S475 (Figure 4D, S4D–E). Thus, CDK13 kinase activity is required for ZC3H14 S475 phosphorylation. *In vitro* kinase reactions (radioactive kinase assay in Figure 4E and labeled ATP immunoblot (53) in Figure S4F) demonstrated CDK13/CCNT1 was able to phosphorylate full-length WT ZC3H14 but not ZC3H14 S475A.

We looked at ZC3H14's binding partners in the presence and absence of CDK13 kinase activity. When ZC3H14 was IPed from CDK13^{mut} cells, fewer binding partners were identified (ZC3H14 peptides were not statistically different) (Figure S4G, row 2–3; Figure S4H, left columns). Total IPed peptides were normalized to total bait (ZC3H14) peptides. Differential binding was calculated between CDK13^{WT} and CDK13^{mut} conditions (t-test p-value <0.05), which identified 18 proteins that required intact CDK13 kinase activity to promote binding to ZC3H14. The three most abundant proteins that required CDK13 kinase activity to promote binding to ZC3H14 were THOC2, ZFC3H1, and MTR4 (Figure 4F, black vs. blue bars) (THOC2 q<0.0001, ZFC3H1 q<0.0001, and MTR4 q=0.018). THOC2 functions in RNA export and binds ZC3H14 (54), ZFC3H1 is a linker between the PAXT and the nuclear RNA degradation machinery, and MTR4 is a helicase required for nuclear RNA degradation (22). We also observed that ZC3H14 bound PAXT proteins PABPN1 and ZC3H18; however binding of these proteins to ZC3H14 was independent of CDK13 kinase activity (Figure 4F). These data show that ZC3H14 binds to multiple PAXT members and that CDK13 kinase activity promotes ZC3H14 binding to THOC2 and two key PAXT components - ZFC3H1 and MTR4.

To test whether the ZC3H14 S475 phosphorylation was sufficient to recruit PAXT binding, phospho-mimetic ZC3H14^{S475D} was tagged, transiently expressed, and IPed from cells lacking CDK13 kinase activity. ZC3H14^{S475D} was sufficient to rescue binding of PAXT components to ZC3H14 (Figure 4F red bars; S4I, fourth row, Figure S4I–J), even in cells lacking CDK13 kinase activity. To test whether ZC3H14 S475 was necessary for PAXT recruitment, non-phosphorylatable ZC3H14^{S475A} was IPed from CDK13^{WT} cells. ZC3H14^{S475A} failed to recruit PAXT components (Figure 4F, yellow bars; S4G last row, Figure S4K–L), even in cells with intact CDK13 kinase activity. The amount of ZC3H14 IPed was statistically unchanged (Figure S4H, right columns). Together, these data show that ZC3H14 S475 phosphorylation promotes PAXT recruitment to ZC3H14.

To test whether ZC3H14 S475 phosphorylation is also necessary and sufficient to activate ptRNA degradation, a two-pronged approach was undertaken. First, short interfering RNAs were used to decrease levels of ZFC3H1 (n=3) or ZC3H14 (n=3), and differential RNA expression was assessed using 3'seq and RNA-seq (Figure S4M) as compared to a scrambled control (n=3). Second, stable human melanoma cell lines expressing non-phosphorylatable ZC3H14^{S475A} (n=2), phospho-mimetic ZC3H14^{S475E} (n=3) or a control protein (n=3) were subjected to RNA-seq (Figure S4N). ZC3H14^{S475E} was used because we were unable to make stable lines with ZC3H14^{S475D}. 3' sequencing from siZFC3H1, siZC3H14, siControl, and prior CDK13^{mut} and control samples were used to build an expression map for ptRNAs and dominant isoforms in human melanoma cells. This ptRNA isoform expression map was used to calculate differential RNA expression using DEXseq

in all conditions as compared to appropriate controls. A boxplot of significantly changed RNAs (q<0.1) from ZFC3H1 vs. control knockdown in human melanoma cells demonstrated an increase in ptRNA isoforms, but minimally changed last exons and constitutive internal exons as expected (Figure 4G, red). siZC3H14 visualized in the same manner showed very few significant expression changes (Figure S4O), which may be due to activity of residual protein or redundancy with another protein. Expression of ZC3H14^{S475A} vs. CLOVER (q<0.1) showed a modest increase in ptRNA expression, while last and constitutive internal exons were minimally changed (Figure 4G, yellow). Expression of ZC3H14^{S475E} vs. CLOVER (q<0.1) caused a decrease in ptRNAs while not affecting last or internal exons (Figure 4G, blue) (Median fold change and wilcoxon rank sum comparing ptRNAs, internal exons, and last exons in Table S5). The *TP53* ptRNA, which is upregulated in CDK13^{mut} cells, was upregulated in ZFC3H1 knockdown, and upon non-phosphorylatable ZC3H14^{S475A}-expression, consistent with loss of PAXT nuclear RNA degradation. In contrast, phospho-mimetic ZC3H14^{S475E} caused lower expression of the *TP53* ptRNA, consistent with hyper-activation of PAXT RNA degradation (Figure 4H). Together these data show that ZC3H14 S475 phosphorylation is necessary and sufficient to activate PAXT to degrade ptRNAs.

To test whether expression of ZC3H14 phosphomimetic and non-phosphorylatable mutants affected human melanoma cell growth rate, doubling time was measured. ZC3H14^{S475A} expressing-cells proliferated at a similar rate to CDK13^{mut}-expressing cells, whereas ZC3H14^{S475E}-expressing cells had an increased doubling time (grew more slowly) (Figure 4I, columns 1–2, 4). These data are consistent with the hypothesis that cells with higher ptRNA levels have an increased growth rate, whereas cells with lower ptRNA expression have a slower growth rate. To determine whether effects of CDK13^{mut} and ZC3H14^{S475} expression function in the same or a parallel ptRNA surveillance pathway, ZC3H14^{S475} phosphomimetic and non-phosphorylatable mutants were expressed in CDK13^{mut} human melanoma cells. We were unable to recover CDK13^{mut} cells that expressed ZC3H14^{S475E}, indicating that CDK13^{mut} cells are addicted to ptRNA expression or that carrying both mutations is deleterious to cell viability. Importantly, CDK13^{mut} +ZC3H14^{S475A} cells had a similar growth rate to either mutant alone (Figure 4I, column 3) and affected the same ptRNAs to a similar magnitude as CDK13^{mut} (Figure S4P–Q). Our data demonstrate that mutant CDK13 expression caused inefficient PAXT recruitment and ptRNA stabilization, supporting an oncogenic role for ptRNAs (Figure S4R).

Prematurely Terminated RNA Accumulation is Oncogenic.

To determine whether *CDK13*^{mut} causes accumulation of ptRNAs in other cancers, publicly available RNA-seq from patient tumor samples from multiple tumor types were examined (bladder, colorectal, lung, melanoma, lung, and uterus). RNA-seq from tumors with CDK13 kinase-domain or nonsense mutations were compared to CDK13^{WT} tumors with matched tumor and patient characteristics (Table S6) using the PAXT-regulated ptRNA isoform map developed for Figure 4. PAXT-regulated ptRNA isoforms are significantly upregulated in CDK13^{mut} cancers, as compared to internal exons (Figure 5A, $p<2.2e^{-16}$). Last exons are also upregulated relative to internal exons, suggesting a general increase in the stability of polyadenylated RNAs in CDK13 mutant tumors (Figure 5A), which may have been

revealed due to the high RNA degradation levels typically observed in patient samples. The CDK13/PAXT target *TP53* ptRNA was more highly expressed in RNA-seq coverage profiles of CDK13 mutant tumors as compared to matched $CDK13^{WT}$ controls (Figure 5B). These data show that patient tumors with CDK13 mutations from many cancer types exhibit an accumulation of PAXT-sensitive ptRNAs.

To test whether ptRNA expression is oncogenic, human *TP53* ptRNA or *SUV39H1* ptRNA vs. control EGFP were expressed in melanocytes in the Triples zebrafish melanoma model. Human *TP53* ptRNA expression caused increased black patches at 7 weeks consistent with early melanoma ($p<0.0001$, two side chi square) (Figure 5C–D, S5A) and expedited melanoma onset ($p=0.0391$) (Figure 5E). Expression of human *SUV39H1* ptRNA also caused increased black patches at 7 weeks ($p=0.0051$) (Figure 5F–G, S5B) and expedited melanoma onset ($p<0001$) (Figure 5H). qPCR confirmed ptRNA expression (Figure S5C–D). As the *TP53* ptRNA is oncogenic and derives from the *TP53* locus, we performed p53 immunoblots and found that $CDK13^{mut}$ human melanoma cells have intact p53 full-length protein (Figure S5E). These data show that human ptRNAs are sufficient to expedite melanoma onset in zebrafish, and more generally that ptRNAs can be oncogenic.

Since loss of PAXT activity may represent a more widespread mechanism of oncogenesis, we probed public databases and found that CDK13-regulated PAXT members are deleted or mutated in 17% of melanomas (Table 2). Analysis with OncodriveFM in melanoma samples found *ZC3H18* is a marginally significant genome-wide driver gene ($q=0.057$; $p=0.0074$); while *ZFC3H1* was not found to be a likely driver ($q=0.22$; $p=0.051$) (Figure S5F–G). The PAXT adaptor protein ZFC3H1 is recurrently mutated (K385Nfs*9) in 23 different patient tumors representing a wide variety of cancers (Figure 5I) and has non-recurrent mutations in 5–11% of multiple cancer types including non-melanoma skin cancer, endometrial cancer, colon adenocarcinoma, and small cell lung cancer (Figure S5H). *ZC3H18* is recurrently mutated (R680Q/Gfs*) in 48 individual samples from a broad variety of cancers (Figure 5J) and has non-recurrent mutations in many cancers including non-melanoma skin cancers, vaginal, and endometrial cancers (Figure S5I). Together these data suggest that nuclear RNA quality control via the PAXT complex is critical to avoid accumulation of prematurely truncated RNAs and their aberrant protein products in multiple cancer types and supports deficient nuclear RNA surveillance as a general oncogenic mechanism.

Discussion

Our data show that *CDK13* has properties consistent with a tumor suppressor whose mutations lead to accumulation of prematurely terminated transcripts by preventing their normal degradation. CDK13 normally phosphorylates ZC3H14 S475, which is necessary and sufficient to promote PAXT recruitment and ptRNA degradation. When CDK13 is mutated, failure to recruit the PAXT complex results in the accumulation of truncated oncogenic transcripts which are exported to the cytoplasm and translated into truncated proteins. Expression of ptRNAs observed in CDK13 mutant melanoma can cause more aggressive cancer. Our data show that mutant CDK13 disrupts a deeply conserved pathway to cause ptRNA accumulation and that ptRNA accumulation is oncogenic.

In the CDK13-associated developmental disorder, de novo CDK13 mutations are thought to work via a dominant negative mechanism. Homozygous CDK13 loss of function causes lethal heart malformations in mice (55) and likely causes embryonic lethality in humans as homozygous deletion is not observed in phenotypically normal people (n=54,980) (56) or in patients with a developmental disorder (n=43,173) (57). Heterozygous *CDK13* deletions have been identified in normal humans in two genomic aggregate databases (gnomAD, Database of Genomic Variants) (19). In contrast, heterozygous *CDK13* kinase domain mutations cause a syndromic developmental disorder that affects heart development as well as other neural crest-derived tissues. Our work raises the possibility that individuals with the *CDK13*-related disorder could be predisposed to developing cancer, which is supported by a recent report of a 9-year-old *CDK13*-related disorder patient developing leukemia (58). The strong mutant *CDK13*-associated disorder phenotypes are more severe than loss of one *CDK13* allele, which supports that CDK13 kinase-domain mutations have dominant negative activity.

Our initial insight for this work came from the observation of that CDK13 mutations in melanoma were enriched in the kinase domain, which suggested a genetic function beyond haploinsufficiency. Our data support a model where CDK13 heterozygous loss of function is selected for (50% activity loss) while heterozygous kinase domain mutations are additionally selected for. This is because non-phosphorylatable CDK13 acts in a dominant negative manner, ie blocks $CDK13^{WT}$ from activating its targets (>50% activity loss). Loss of both alleles is infrequently observed, possibly due to reduced cellular fitness as was seen for a cancer cell line (59). We supposed that CDK13 kinase-domain mutations cause a more severe PAXT deficiency and thus are more selected for than mutations that cause CDK13 haploinsufficiency. Our zebrafish genetics and the lack of CDK13 mutations in melanoma Cyclin-binding residues suggested that $CDK13^{mut}$ dominant negative activity requires Cyclin binding. Expression of $CDK13^{mut}$ in a $CDK13^{WT}$ background recapitulated the RNA cancer phenotypes observed in melanoma patients with heterozygous CDK13 mutations. In multiple CDK13 experimental systems, we found that mutant CDK13 causes the same RNA and cancer phenotype, namely accumulated ptRNAs and more aggressive melanoma. We hypothesized that, only by modeling the human genetics and chronically expressing kinase-mutant CDK13 in the presence of $CDK13^{WT}$, we would be able to uncover CDK13's role in RNA surveillance. Our work shows that CDK13's function in ptRNA degradation is utilized broadly.

ptRNAs in $CDK13^{mut}$ cells are exported and translated into truncated proteins. Transcripts that terminate via intronic polyadenylation sites are predicted to be exported and translated if they escape nuclear decay (21, 45). We are not aware of any studies documenting proteome-wide measurements of ptRNA translation including intronic sequences. Large-scale truncated protein expression would be predicted to cause protein stress in cells, which is consistent with the observed upregulation of autophagic and lysosomal proteins in CDK13 mutated melanomas. Of potentially great importance for predicting immunotherapy responses in patients, we found evidence that the truncated proteins can end in translated intronic sequences. Translated intronic sequences have the potential to produce neoantigens that would be absent from $CDK13^{WT}$ cells and thus would be predicted to elicit a highly tumor-specific immune response.

ptRNAs derived from intronic polyadenylation sites are enriched in cancers (60). We hypothesize that different cancers will accumulate different ptRNAs depending on the RNAs expressed and the mechanism of ptRNA accumulation. Loss-of-function mutations in CDK12 in metastatic castration-resistant prostate cancer and serous ovarian carcinomas cause increased production of truncated RNAs in DNA repair genes (7, 8), contributing to CDK12's tumor suppressive properties. The IPA sites upregulated by CDK12 loss appear to be mostly but not fully distinct from those seen when CDK13 is lost (Figure S2E, Data S1), consistent with CDK12 and CDK13 having divergent mechanisms of ptRNA regulation.

Widespread ptRNA formation has also been reported to take place when the U1 snRNA is prevented from pairing with 5' splice sites, in a phenomenon called "telescripting" (61). Interestingly, the U1 spliceosomal RNA is recurrently mutated in multiple cancers at base 3 which pairs with the 5' splice site (62). This mutationis predicted to cause increased generation of ptRNAs and could represent a third mechanism by which ptRNA expression promotes oncogenesis. We envision mechanisms that govern 3' end formation, such as telescripting and those that govern ptRNA stability such as CDK13 as complementary ptRNA control mechanisms. It will be important to investigate expression of ptRNAs and other aberrant RNAs in different cancers with different driver mutations as aberrant RNA accumulation could represent a final common pathway.

Germline mutations in PAXT-associated proteins ZC3H14 and THOC2 cause a neurodevelopmental disorder (51, 63), suggesting that the regulation of prematurely terminated RNAs in the nucleus has broad implications in development and disease. We propose that loss of nuclear RNA surveillance via CDK13 and PAXT is a general oncogenic mechanism. PAXT members regulated by CDK13 are mutated in 17% of melanomas in addition to the 3.9% of melanomas harboring CDK13 mutations, raising the possibility that loss of nuclear surveillance is a contributing factor in up to 21% of melanoma. We showed that patients with other malignancies harboring CDK13 mutations also accumulate prematurely terminated RNAs. We also found that recurrent mutations in key PAXT members *ZFC3H1* and *ZC3H18* occur in many cancers, implying that these mutations may potentially be selected for; further work will be required to support this hypothesis. The finding that mutant *CDK13* is oncogenic via deficient RNA surveillance and that recurrent mutations occur in multiple PAXT components suggests a broad, previously unrecognized tumor suppressive role for nuclear RNA surveillance.

Supplementary Material

Refer to Web version on PubMed Central for supplementary material.

Acknowledgements.

The CDK13 antibody used for mouse experiments and to detect truncated CDK13 was a gift from A.L. Greenleaf. The pAC4 and PBNeoTetO-Dest vectors were gifts from A. Cheng. We acknowledge the Harvard Nascent Transcriptomics Core for assistance with TT-seq. The human cancer cell template used in Figure S4 was adapted from BioRender. Analyses presented here are in part based upon data generated by the TCGA Research Network: https://www.cancer.gov/tcga. This work utilized the Biowulf cluster computing system at the NIH.

Funding.

This research was supported by Damon Runyon Cancer Foundation Fellowship Award (M.I.), American Society of Clinical Oncology Young Investigator Award (M.I.), T32HL116324 from the National Heart, Lung, and Blood Institute (M.I.), NCI K08CA248727 (M.I.), Charles S Memorial Sloan Kettering Starr Foundation Cancer Consortium, The Hope Funds for Cancer Research Grillo-Marxuach Family Fellowship (B.J.A.), The American Lebanese Syrian Associated Charities (ALSAC) (B.J.A.), R01CA103846 (L.I.Z.), NIH R01GM141544 (P.L.B.), a University of Rochester Health Sciences Center for Computational Innovation high performance computational resource grant (P.L.B.), a David H. Koch Fellowship (S.J.D.), NIH T32 GM135134 (D.E.E.), NIH R35 GM144283 (R.A.Y.), and the Ludwig Center at Harvard (K.A. and B.E.J.M.). P.A.S., S.J.D, and P.B. were supported by NIH P01CA042063, NIH R01GM034277, and NIH R01CA133404. M.G. is funded by the Deutsche Forschungsgemeinschaft under Germany's Excellence Strategy – EXC2151 – 390873048 and grant (GE 976/9-2). This work has also been supported by the Intramural Research Program (IRP) of the Division of Cancer Epidemiology and Genetics, National Cancer Institute, US National Institutes of Health (TZ, KMB, SJC).

Data and materials availability:

The datasets generated during and/or analyzed during the current study are uploaded to GEO (Superseries GSE131334). Newly generated code was deposited here: https://zenodo.org/badge/latestdoi/577358557. The TCGA patient RNA-seq bams are controlled-access data with unique identifiers so they cannot be publicly shared. All zebrafish strains, cell lines, and DNA vectors are readily available via contact of the corresponding author. Where possible, we can share remaining zebrafish tumor material, however this material is limited in abundance. All antibodies are commercially available.

References and notes

1. Hydbring P, Malumbres M, Sicinski P, Non-canonical functions of cell cycle cyclins and cyclin-dependent kinases. Nat Rev Mol Cell Biol 17, 280–292 (2016). [PubMed: 27033256]
2. Malumbres M, Cyclin-dependent kinases. Genome Biol 15, 122 (2014). [PubMed: 25180339]
3. Adelman K, Lis JT, Promoter-proximal pausing of RNA polymerase II: emerging roles in metazoans. Nat Rev Genet 13, 720–731 (2012). [PubMed: 22986266]
4. McCracken S et al. , 5'-Capping enzymes are targeted to pre-mRNA by binding to the phosphorylated carboxy-terminal domain of RNA polymerase II. Genes Dev 11, 3306–3318 (1997). [PubMed: 9407024]
5. Schwartz BE, Larochelle S, Suter B, Lis JT, Cdk7 is required for full activation of Drosophila heat shock genes and RNA polymerase II phosphorylation in vivo. Mol Cell Biol 23, 6876–6886 (2003). [PubMed: 12972606]
6. Shim EY, Walker AK, Shi Y, Blackwell TK, CDK-9/cyclin T (P-TEFb) is required in two postinitiation pathways for transcription in the C. elegans embryo. Genes Dev 16, 2135–2146 (2002). [PubMed: 12183367]
7. Dubbury SJ, Boutz PL, Sharp PA, CDK12 regulates DNA repair genes by suppressing intronic polyadenylation. Nature 564, 141–145 (2018). [PubMed: 30487607]
8. Krajewska M et al. , CDK12 loss in cancer cells affects DNA damage response genes through premature cleavage and polyadenylation. Nat Commun 10, 1757 (2019). [PubMed: 30988284]
9. Rimel JK et al. , Selective inhibition of CDK7 reveals high-confidence targets and new models for TFIIH function in transcription. Genes Dev 34, 1452–1473 (2020). [PubMed: 33060135]
10. Chipumuro E et al. , CDK7 inhibition suppresses super-enhancer-linked oncogenic transcription in MYCN-driven cancer. Cell 159, 1126–1139 (2014). [PubMed: 25416950]
11. Christensen CL et al. , Targeting transcriptional addictions in small cell lung cancer with a covalent CDK7 inhibitor. Cancer Cell 26, 909–922 (2014). [PubMed: 25490451]
12. Kwiatkowski N et al. , Targeting transcription regulation in cancer with a covalent CDK7 inhibitor. Nature 511, 616–620 (2014). [PubMed: 25043025]
13. Wang Y et al. , CDK7-dependent transcriptional addiction in triple-negative breast cancer. Cell 163, 174–186 (2015). [PubMed: 26406377]

14. Sheppard HE et al. , Targeted brachyury degradation disrupts a highly specific autoregulatory program controlling chordoma cell identity. Cell Rep Med 2, 100188 (2021). [PubMed: 33521702]
15. S. Deciphering Developmental Disorders, Prevalence and architecture of de novo mutations in developmental disorders. Nature 542, 433–438 (2017). [PubMed: 28135719]
16. Sifrim A et al. , Distinct genetic architectures for syndromic and nonsyndromic congenital heart defects identified by exome sequencing. Nat Genet 48, 1060–1065 (2016). [PubMed: 27479907]
17. van den Akker WMR et al. , De novo variants in CDK13 associated with syndromic ID/DD: Molecular and clinical delineation of 15 individuals and a further review. Clin Genet 93, 1000–1007 (2018). [PubMed: 29393965]
18. Bostwick BL et al. , Phenotypic and molecular characterisation of CDK13-related congenital heart defects, dysmorphic facial features and intellectual developmental disorders. Genome Med 9, 73 (2017). [PubMed: 28807008]
19. Hamilton MJ et al. , Heterozygous mutations affecting the protein kinase domain of CDK13 cause a syndromic form of developmental delay and intellectual disability. J Med Genet 55, 28–38 (2018). [PubMed: 29021403]
20. Gu B, Eick D, Bensaude O, CTD serine-2 plays a critical role in splicing and termination factor recruitment to RNA polymerase II in vivo. Nucleic Acids Res 41, 1591–1603 (2013). [PubMed: 23275552]
21. Spraggon L, Cartegni L, U1 snRNP-Dependent Suppression of Polyadenylation: Physiological Role and Therapeutic Opportunities in Cancer. Int J Cell Biol 2013, 846510 (2013). [PubMed: 24285958]
22. Meola N et al. , Identification of a Nuclear Exosome Decay Pathway for Processed Transcripts. Mol Cell 64, 520–533 (2016). [PubMed: 27871484]
23. Ogami K et al. , An Mtr4/ZFC3H1 complex facilitates turnover of unstable nuclear RNAs to prevent their cytoplasmic transport and global translational repression. Genes Dev 31, 1257–1271 (2017). [PubMed: 28733371]
24. Hoadley KA et al. , Cell-of-Origin Patterns Dominate the Molecular Classification of 10,000 Tumors from 33 Types of Cancer. Cell 173, 291–304 e296 (2018). [PubMed: 29625048]
25. N. Cancer Genome Atlas, Genomic Classification of Cutaneous Melanoma. Cell 161, 1681–1696 (2015). [PubMed: 26091043]
26. Liu D et al. , Integrative molecular and clinical modeling of clinical outcomes to PD1 blockade in patients with metastatic melanoma. Nat Med 25, 1916–1927 (2019). [PubMed: 31792460]
27. Hugo W et al. , Genomic and Transcriptomic Features of Response to Anti-PD-1 Therapy in Metastatic Melanoma. Cell 165, 35–44 (2016). [PubMed: 26997480]
28. Snyder A et al. , Genetic basis for clinical response to CTLA-4 blockade in melanoma. N Engl J Med 371, 2189–2199 (2014). [PubMed: 25409260]
29. Van Allen EM et al. , Genomic correlates of response to CTLA-4 blockade in metastatic melanoma. Science 350, 207–211 (2015). [PubMed: 26359337]
30. Hodis E et al. , A landscape of driver mutations in melanoma. Cell 150, 251–263 (2012). [PubMed: 22817889]
31. Krauthammer M et al. , Exome sequencing identifies recurrent somatic RAC1 mutations in melanoma. Nat Genet 44, 1006–1014 (2012). [PubMed: 22842228]
32. Van Allen EM et al. , The genetic landscape of clinical resistance to RAF inhibition in metastatic melanoma. Cancer Discov 4, 94–109 (2014). [PubMed: 24265153]
33. Hayward NK et al. , Whole-genome landscapes of major melanoma subtypes. Nature 545, 175–180 (2017). [PubMed: 28467829]
34. Gonzalez-Perez A, Lopez-Bigas N, Functional impact bias reveals cancer drivers. Nucleic Acids Res 40, e169 (2012). [PubMed: 22904074]
35. Greifenberg AK et al. , Structural and Functional Analysis of the Cdk13/Cyclin K Complex. Cell Rep 14, 320–331 (2016). [PubMed: 26748711]
36. Carrera AC, Alexandrov K, Roberts TM, The conserved lysine of the catalytic domain of protein kinases is actively involved in the phosphotransfer reaction and not required for anchoring ATP. Proc Natl Acad Sci U S A 90, 442–446 (1993). [PubMed: 8421674]

37. Ablain J et al. , Human tumor genomics and zebrafish modeling identify SPRED1 loss as a driver of mucosal melanoma. Science 362, 1055–1060 (2018). [PubMed: 30385465]
38. Ceol CJ et al. , The histone methyltransferase SETDB1 is recurrently amplified in melanoma and accelerates its onset. Nature 471, 513–517 (2011). [PubMed: 21430779]
39. Patton EE et al. , BRAF mutations are sufficient to promote nevi formation and cooperate with p53 in the genesis of melanoma. Curr Biol 15, 249–254 (2005). [PubMed: 15694309]
40. Blazek D et al. , The Cyclin K/Cdk12 complex maintains genomic stability via regulation of expression of DNA damage response genes. Genes Dev 25, 2158–2172 (2011). [PubMed: 22012619]
41. Liang K et al. , Characterization of human cyclin-dependent kinase 12 (CDK12) and CDK13 complexes in C-terminal domain phosphorylation, gene transcription, and RNA processing. Mol Cell Biol 35, 928–938 (2015). [PubMed: 25561469]
42. Dai Q et al. , Cyclin K-containing kinase complexes maintain self-renewal in murine embryonic stem cells. J Biol Chem 287, 25344–25352 (2012). [PubMed: 22547058]
43. Anders S, Reyes A, Huber W, Detecting differential usage of exons from RNA-seq data. Genome Res 22, 2008–2017 (2012). [PubMed: 22722343]
44. Schwalb B et al. , TT-seq maps the human transient transcriptome. Science 352, 1225–1228 (2016). [PubMed: 27257258]
45. Silla T, Karadoulama E, Makosa D, Lubas M, Jensen TH, The RNA Exosome Adaptor ZFC3H1 Functionally Competes with Nuclear Export Activity to Retain Target Transcripts. Cell Rep 23, 2199–2210 (2018). [PubMed: 29768216]
46. Khyrul WA, LaLonde DP, Brown MC, Levinson H, Turner CE, The integrin-linked kinase regulates cell morphology and motility in a rho-associated kinase-dependent manner. J Biol Chem 279, 54131–54139 (2004). [PubMed: 15485819]
47. May MJ, Marienfeld RB, Ghosh S, Characterization of the Ikappa B-kinase NEMO binding domain. J Biol Chem 277, 45992–46000 (2002). [PubMed: 12244103]
48. Lian CG et al. , Loss of 5-hydroxymethylcytosine is an epigenetic hallmark of melanoma. Cell 150, 1135–1146 (2012). [PubMed: 22980977]
49. Ashburner M et al. , Gene ontology: tool for the unification of biology. The Gene Ontology Consortium. Nat Genet 25, 25–29 (2000). [PubMed: 10802651]
50. Wu G et al. , A Two-Layered Targeting Mechanism Underlies Nuclear RNA Sorting by the Human Exosome. Cell Rep 30, 2387–2401 e2385 (2020). [PubMed: 32075771]
51. Pak C et al. , Mutation of the conserved polyadenosine RNA binding protein, ZC3H14/dNab2, impairs neural function in Drosophila and humans. Proc Natl Acad Sci U S A 108, 12390–12395 (2011). [PubMed: 21734151]
52. Rha J et al. , The RNA-binding protein, ZC3H14, is required for proper poly(A) tail length control, expression of synaptic proteins, and brain function in mice. Hum Mol Genet 26, 3663–3681 (2017). [PubMed: 28666327]
53. Allen JJ et al. , A semisynthetic epitope for kinase substrates. Nat Methods 4, 511–516 (2007). [PubMed: 17486086]
54. Morris KJ, Corbett AH, The polyadenosine RNA-binding protein ZC3H14 interacts with the THO complex and coordinately regulates the processing of neuronal transcripts. Nucleic Acids Res 46, 6561–6575 (2018). [PubMed: 29912477]
55. Novakova M et al. , Mouse Model of Congenital Heart Defects, Dysmorphic Facial Features and Intellectual Developmental Disorders as a Result of Non-functional CDK13. Front Cell Dev Biol 7, 155 (2019). [PubMed: 31440507]
56. MacDonald JR, Ziman R, Yuen RK, Feuk L, Scherer SW, The Database of Genomic Variants: a curated collection of structural variation in the human genome. Nucleic Acids Res 42, D986–992 (2014). [PubMed: 24174537]
57. Firth HV et al. , DECIPHER: Database of Chromosomal Imbalance and Phenotype in Humans Using Ensembl Resources. Am J Hum Genet 84, 524–533 (2009). [PubMed: 19344873]
58. Cui D, Wang S, Zhang A, Liu A, Hu Q, Case Report: Hemophagocytic Lymphohistiocytosis Prior to the Onset of Leukemia in a Boy With CDK13-Related Disorder. Front Genet 13, 858668 (2022). [PubMed: 35651941]

59. Fan Z et al. , CDK13 cooperates with CDK12 to control global RNA polymerase II processivity. Sci Adv 6, (2020).
60. Lee SH et al. , Widespread intronic polyadenylation inactivates tumour suppressor genes in leukaemia. Nature 561, 127–131 (2018). [PubMed: 30150773]
61. So BR et al. , A Complex of U1 snRNP with Cleavage and Polyadenylation Factors Controls Telescripting, Regulating mRNA Transcription in Human Cells. Mol Cell 76, 590–599 e594 (2019). [PubMed: 31522989]
62. Shuai S et al. , The U1 spliceosomal RNA is recurrently mutated in multiple cancers. Nature 574, 712–716 (2019). [PubMed: 31597163]
63. Kumar R et al. , THOC2 Mutations Implicate mRNA-Export Pathway in X-Linked Intellectual Disability. Am J Hum Genet 97, 302–310 (2015). [PubMed: 26166480]
64. Viswanathan SR et al. , Structural Alterations Driving Castration-Resistant Prostate Cancer Revealed by Linked-Read Genome Sequencing. Cell 174, 433–447 e419 (2018). [PubMed: 29909985]
65. Cancer N Genome Atlas Research, Integrated genomic analyses of ovarian carcinoma. Nature 474, 609–615 (2011). [PubMed: 21720365]
66. Ekumi KM et al. , Ovarian carcinoma CDK12 mutations misregulate expression of DNA repair genes via deficient formation and function of the Cdk12/CycK complex. Nucleic Acids Res 43, 2575–2589 (2015). [PubMed: 25712099]
67. Adzhubei IA et al. , A method and server for predicting damaging missense mutations. Nat Methods 7, 248–249 (2010). [PubMed: 20354512]
68. Reva B, Antipin Y, Sander C, Predicting the functional impact of protein mutations: application to cancer genomics. Nucleic Acids Res 39, e118 (2011). [PubMed: 21727090]
69. Cerami E et al. , The cBio cancer genomics portal: an open platform for exploring multidimensional cancer genomics data. Cancer Discov 2, 401–404 (2012). [PubMed: 22588877]
70. Li H et al. , The Sequence Alignment/Map format and SAMtools. Bioinformatics 25, 2078–2079 (2009). [PubMed: 19505943]
71. Anders S, Pyl PT, Huber W, HTSeq--a Python framework to work with high-throughput sequencing data. Bioinformatics 31, 166–169 (2015). [PubMed: 25260700]
72. Reyes A et al. , Drift and conservation of differential exon usage across tissues in primate species. Proc Natl Acad Sci U S A 110, 15377–15382 (2013). [PubMed: 24003148]
73. Robinson JT et al. , Integrative genomics viewer. Nat Biotechnol 29, 24–26 (2011). [PubMed: 21221095]
74. Kaufman CK et al. , A zebrafish melanoma model reveals emergence of neural crest identity during melanoma initiation. Science 351, aad2197 (2016). [PubMed: 26823433]
75. Labun K, Montague TG, Gagnon JA, Thyme SB, Valen E, CHOPCHOP v2: a web tool for the next generation of CRISPR genome engineering. Nucleic Acids Res 44, W272–276 (2016). [PubMed: 27185894]
76. Montague TG, Cruz JM, Gagnon JA, Church GM, Valen E, CHOPCHOP: a CRISPR/Cas9 and TALEN web tool for genome editing. Nucleic Acids Res 42, W401–407 (2014). [PubMed: 24861617]
77. Lee TI, Johnstone SE, Young RA, Chromatin immunoprecipitation and microarray-based analysis of protein location. Nat Protoc 1, 729–748 (2006). [PubMed: 17406303]
78. Langmead B, Trapnell C, Pop M, Salzberg SL, Ultrafast and memory-efficient alignment of short DNA sequences to the human genome. Genome Biol 10, R25 (2009). [PubMed: 19261174]
79. Kim D et al. , TopHat2: accurate alignment of transcriptomes in the presence of insertions, deletions and gene fusions. Genome Biol 14, R36 (2013). [PubMed: 23618408]
80. Trapnell C et al. , Differential gene and transcript expression analysis of RNA-seq experiments with TopHat and Cufflinks. Nat Protoc 7, 562–578 (2012). [PubMed: 22383036]
81. Dobin A et al. , STAR: ultrafast universal RNA-seq aligner. Bioinformatics 29, 15–21 (2013). [PubMed: 23104886]
82. Quinlan AR, Hall IM, BEDTools: a flexible suite of utilities for comparing genomic features. Bioinformatics 26, 841–842 (2010). [PubMed: 20110278]

83. Campeau E et al. , A versatile viral system for expression and depletion of proteins in mammalian cells. PLoS One 4, e6529 (2009). [PubMed: 19657394]

84. Bray NL, Pimentel H, Melsted P, Pachter L, Near-optimal probabilistic RNA-seq quantification. Nat Biotechnol 34, 525–527 (2016). [PubMed: 27043002]

85. Cong L et al. , Multiplex genome engineering using CRISPR/Cas systems. Science 339, 819–823 (2013). [PubMed: 23287718]

86. R. C. Team, R: A language and environment for statistical computing. R Foundation for Statistical Computing, Vienna, Austria., (2020).

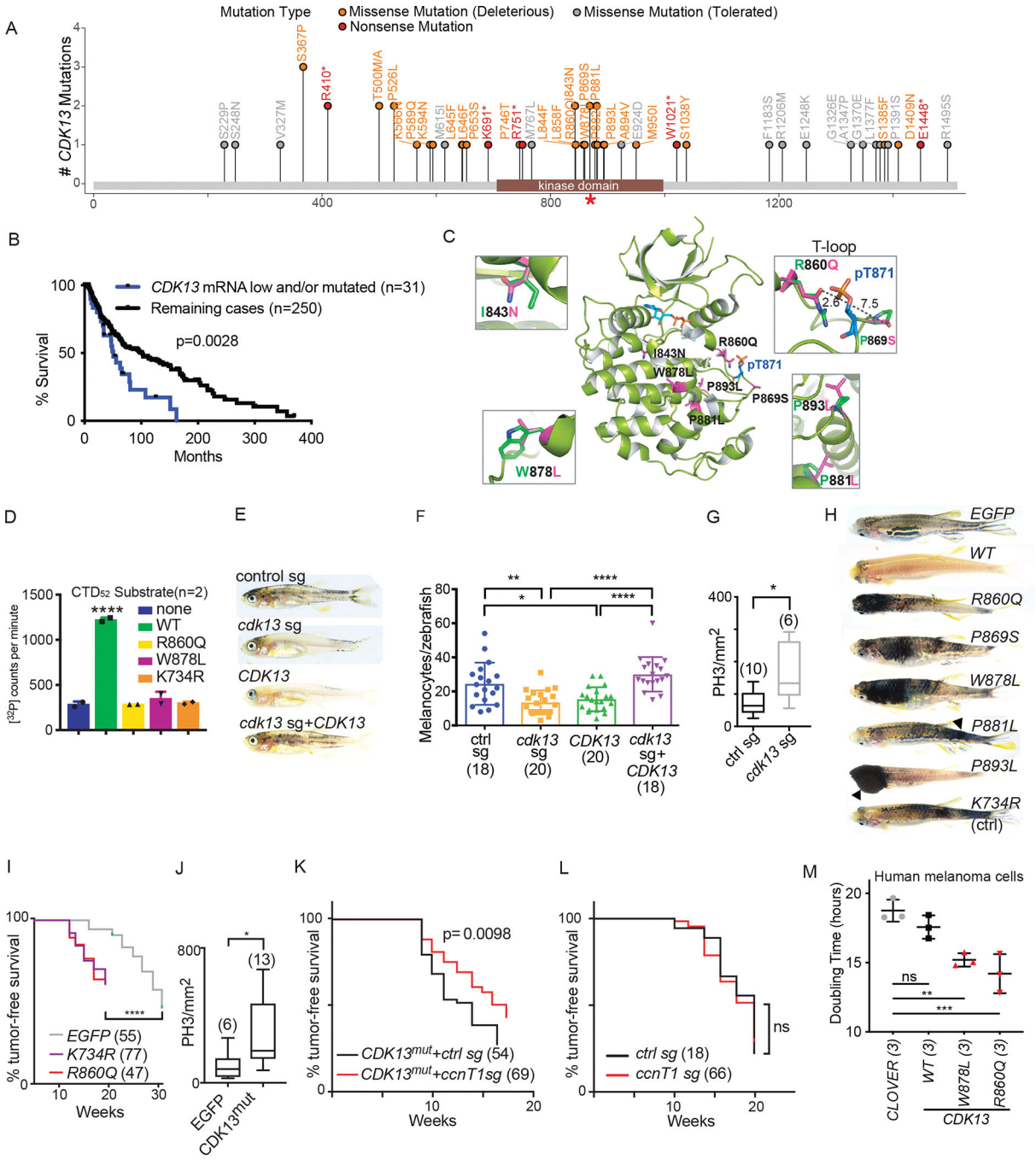

Figure 1: CDK13 has properties consistent with a tumor suppressor.

A) *CDK13* melanoma mutation plot. red *=phosphorylation site. B) Patient survival plot with *CDK13* mutation or downregulation vs. remaining patients. p=0.0028 Log-rank. n= patients. C) Patient kinase-domain mutations mapped on the CDK13 crystal structure. pT871=phosphorylation site. D) *In vitro* kinase assay of wild-type and patient-mutated CDK13 using full-length CTD_{52} as the substrate. One-way ANOVA with no kinase vs. all conditions; WT CDK13 ****=q=0.0001, all other comparisons non-significant. Mean +SD. E) Representative photos of *mitfa:BRAF^{V600E}; p53−/−; mitfa−/−* (Triples melanoma model

zebrafish) with 1) control guide RNA (gRNA), 2) *cdk13* gRNA, 3) human $CDK13^{WT}$, or *cdk13* gRNA and human $CDK13^{WT}$ at 4 weeks post-fertilization. F) Quantification of melanocytes at 3 days post-fertilization for Triples zebrafish injected with 1) control gRNA, 2) *cdk13* gRNA, 3) human $CDK13^{WT}$, or *cdk13* gRNA and human $CDK13^{WT}$. p=one-way ANOVA, multiple comparisons. Mean +/− SD. *= q=0.0186, **=q=0.0030, ****=q<0.0001. (N)=zebrafish. G) Phospho Histone H3 Serine 10 (PH3) antibody staining/mm^2 of melanomas from Triples zebrafish injected with *cdk13* gRNA compared with control gRNA. p=0.014 (Mann Whitney two-tailed t test). (N)=melanomas. H) 9-week photos of melanocyte-specific expression of EGFP, human $CDK13^{WT}$, patient-mutant CDK13, or $CDK13^{K734R}$ (catalytically dead control) in Triples zebrafish. Arrows=melanomas. I) % melanoma-free survival of Triples zebrafish with melanocyte-specific expression of EGFP, $CDK13^{R860Q}$ *(*patient mutation), and $CDK13^{K734R}$ *(*catalytically dead). ****=p<0.0001 (log-rank). (n)=zebrafish. J) PH3 antibody staining/mm^2 of melanoma from Triples zebrafish expressing EGFP vs. CDK13 mutant (W878L or P893L*)*. p=0.0125 (Mann Whitney test, two-tailed). (n)=melanomas. K) Melanoma-free survival of zebrafish with melanocyte-specific expression of $CDK13^{W878L}$ with melanocyte-specific CRISPR of either a control gene or *ccnT1*. p=0.0098 (log-rank). (n)=zebrafish. L) Melanoma-free survival of zebrafish with melanocyte-specific CRISPR of a control gene or *ccnT1* alone. ns=non-significant (log-rank). (n)=zebrafish. M) Doubling time for human melanoma cells expressing CLOVER, $CDK13^{WT}$, $CDK13^{W878L}$, or $CDK13^{R860Q}$. One-way ANOVA with CLOVER vs. all conditions. $CDK13^{W878L}$ q=0.0044, $CDK13^{R860Q}$ q=0.0009. ns = non-significant. Mean +/−SD. n=3 biologic replicates. All box plots with box demonstrating the 25–75 percentile range, solid line represents median, and whiskers show max to min.

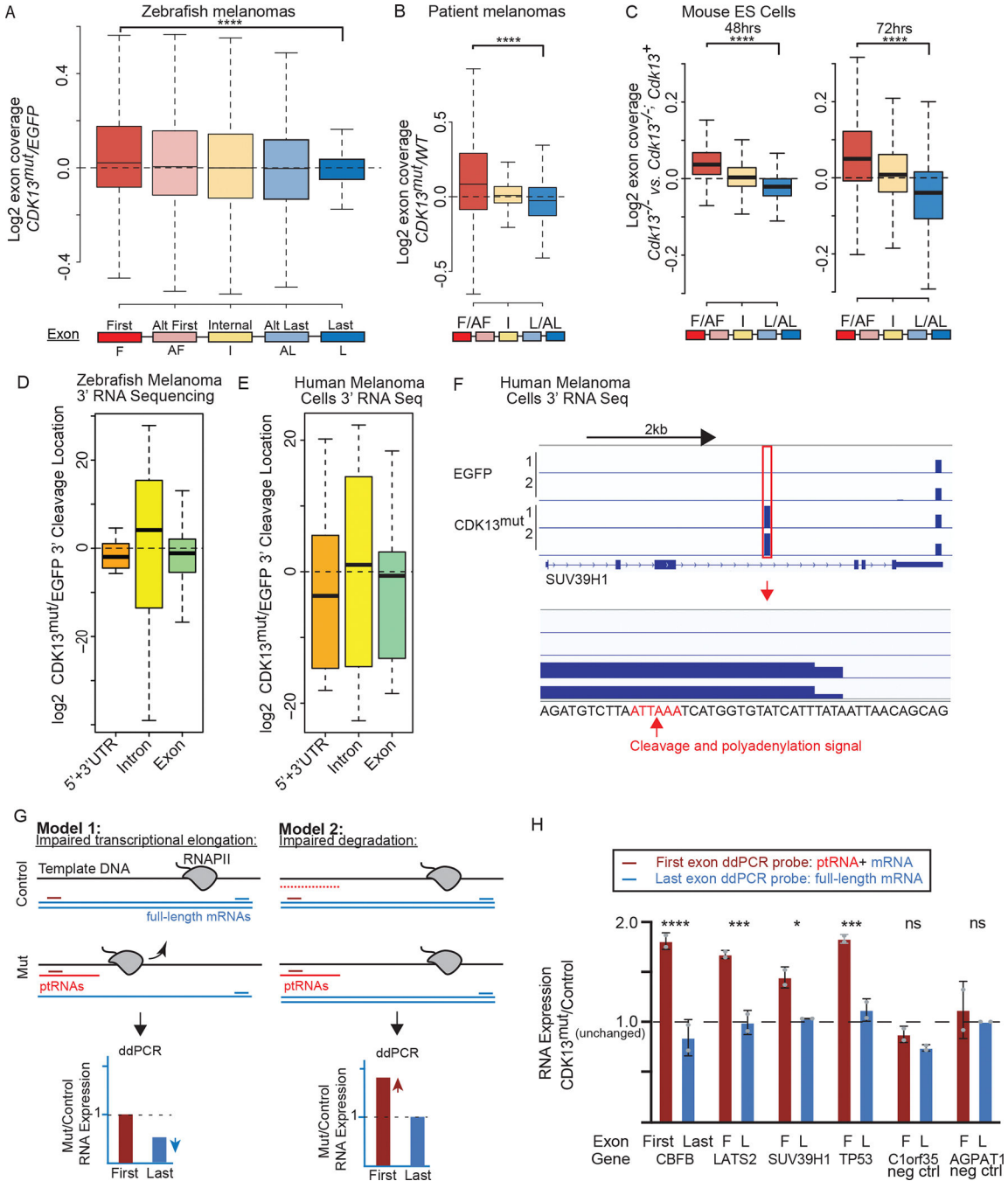

Figure 2: CDK13 mutation results in accumulation of RNAs that prematurely terminate in introns.

A) log2-fold normalized exon expression in CDK13^{R860Q}-(n=5) vs. EGFP-(n=4) expressing zebrafish melanomas. ****=p<2.2×10−16, first vs. last exon. B) log2-fold normalized exon expression for CDK13^{mut} (n=3) vs. CDK13^{WT} (n=5) matched control patient melanomas. ****=p<2.2×10−16, F/AF vs. L/AL exon. C) log2-fold normalized exon expression in Cdk13−/− vs. Cdk13−/−; Cdk13+ (control) mouse embryonic stem (ES) cells. 48 and 72 hours = hours of Cdk13 depletion (n=4 for each). ****=p<2.2×10−16, F/AF vs. L/AL exon. D-E) log2-fold CDK13^{mut}/control cleavage site utilization (3' seq) in UTRs, introns, and

exons. D) Zebrafish melanomas and E) human melanoma cells. F) Integrative Genomics Viewer plot of 3' sequencing showing increased *SUV39H1* ptRNA in $CDK13^{mut}$-expressing vs. control human melanoma cells. Red box indicates the ptRNA 3' end. G) Models for ptRNA accumulation in $CDK13^{mut}$ cells. H) RNA expression in $CDK13^{mut}$/control human melanoma cells measured by digital droplet PCR for 4 genes with increased ptRNAs by 3' sequencing and 2 control genes. F= first exon. L = last exon. 2-way ANOVA, multiple comparisons. adjusted p-values from left to right= **** <0.0001, ***=0.0006, * = 0.0280, ***=0.0004, ns=0.8626, ns=0.9158. +/− SD. In box plots, the black horizontal line indicates the median and whiskers extend to 1.5 × the interquartile range (IQR). p-values A-C = two-sided Wilcoxon rank sum tests.

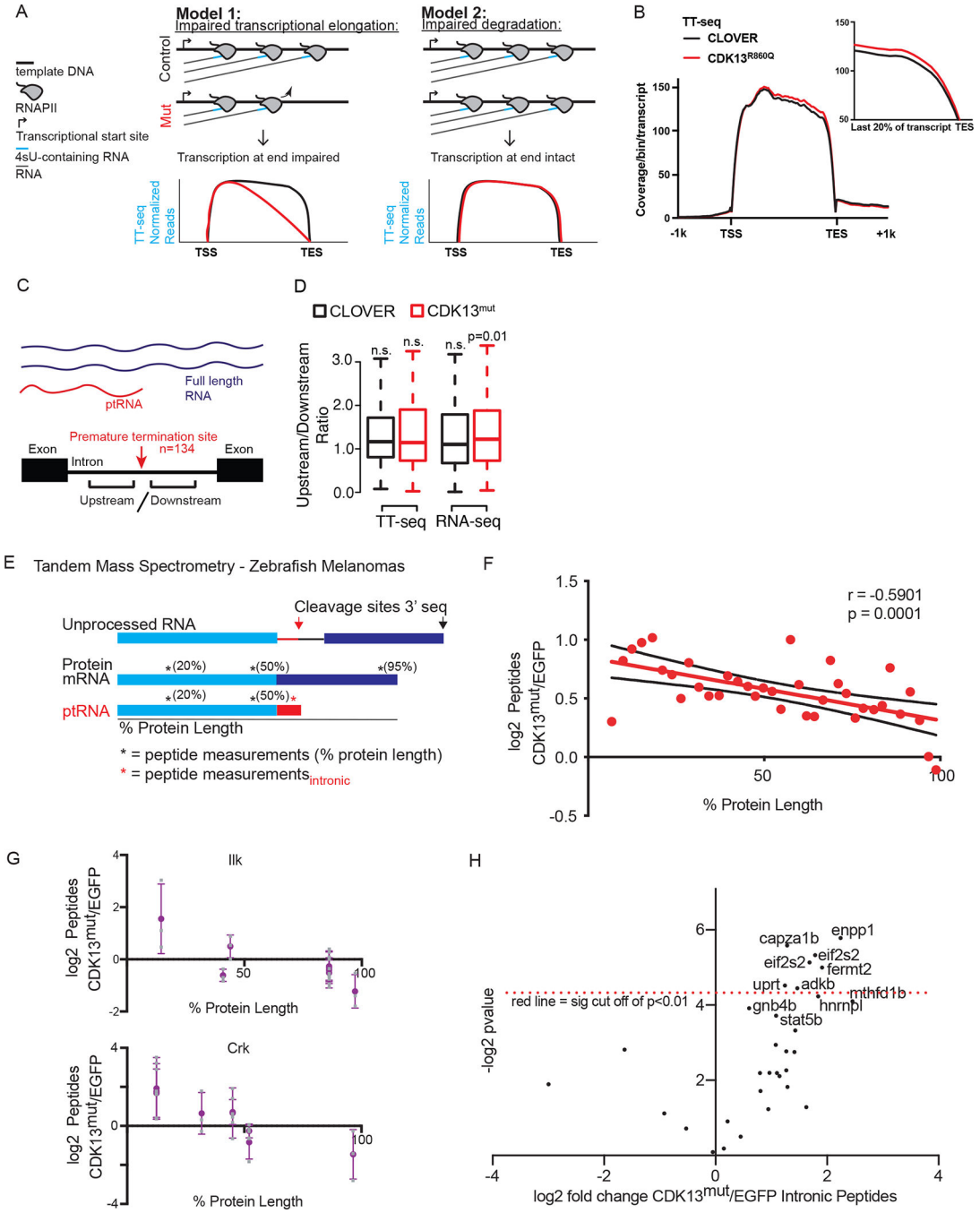

Figure 3: Prematurely terminated RNAs accumulate post-transcriptionally and are translated - including intronic sequences.

A) Models for ptRNA accumulation as measured by Transient Transcriptome Sequencing (TT-seq). TSS = transcriptional start site. TES = transcriptional end site. B) Metagene plots are shown for TT-seq coverage over exons within non-overlapping transcripts from expressed genes (n = 7452) from CDK13^{mut} vs. CLOVER-expressing human melanoma cells. TSS to TES regions are shown, flanked +/− 1kb genomic sequence. C) Schematic for analysis of TT-seq and RNA-seq coverage around intronic polyadenylation sites. D) Box plots of the ratio of upstream (−300 to −1 nt) to downstream (+1 to +300 nt) read coverage

at the 3’ cleavage locations as schematized in C). P-values by Wilcoxon Signed Rank Test compared to the median ratio from all samples. E) Schema of tandem mass spectrometry data analysis from CDK13^{mut}- vs. EGFP-expressing zebrafish melanomas. F) Log2 peptide summed signal to noise (SSN) CDK13^{mut}- vs. EGFP-expressing zebrafish melanomas plotted across a normalized protein length. n=3 zebrafish melanomas each condition. Black lines = 95% confidence intervals. G) Log2 CDK13^{mut}- vs. EGFP-expressing zebrafish melanoma peptide measurements plotted by % protein length for significantly affected proteins for Ilk (upper) and Crk (lower). Gray squares = individual measurements. Error bars = SD. H) Log2 intronic peptides SSN from CDK13^{mut}- vs. EGFP-expressing zebrafish melanomas as predicted from 3’ sequencing on the horizontal axis plotted by −log p-value on the vertical axis (t-test, two tailed). Labels = enriched intronic peptides.

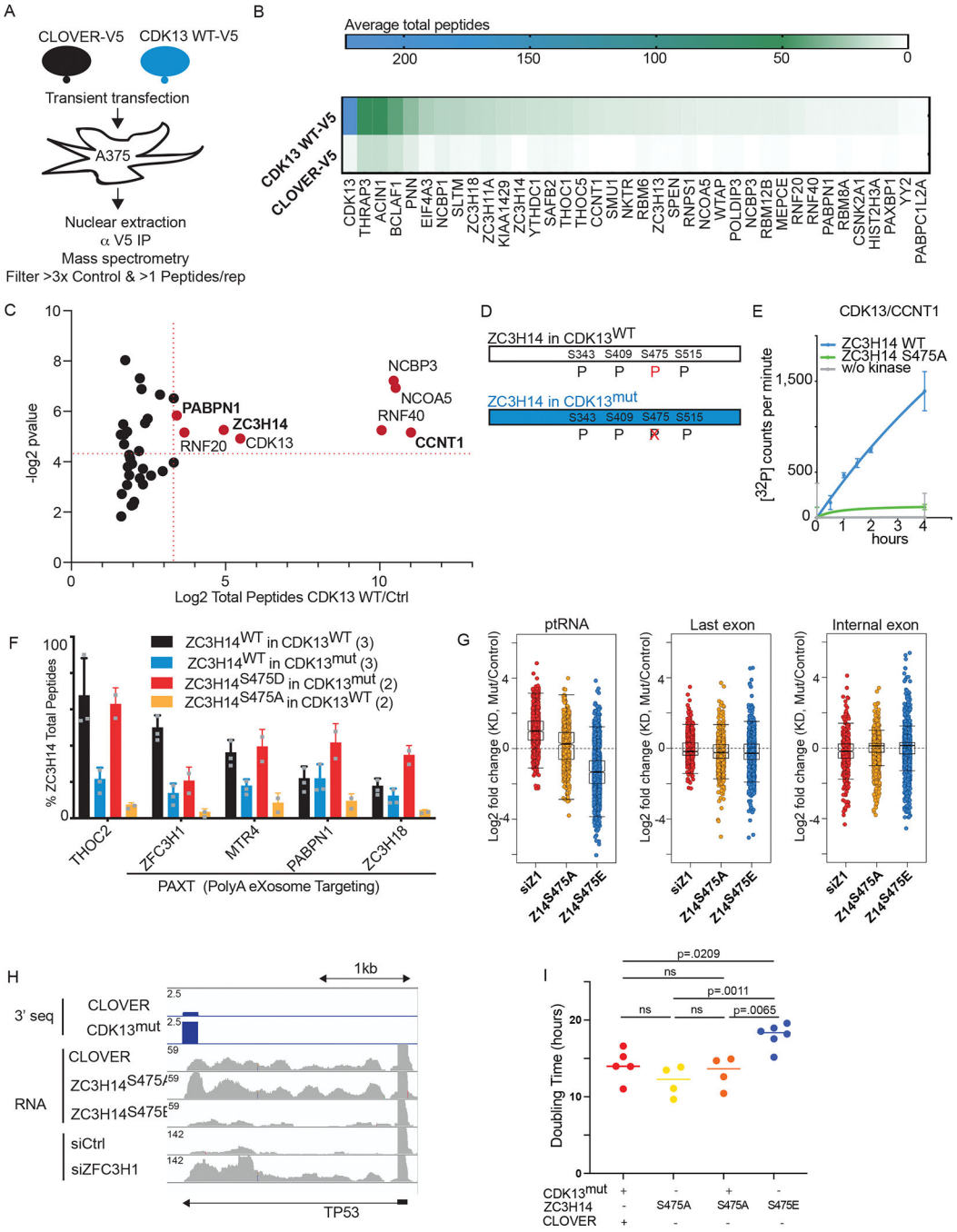

Figure 4: Mutant CDK13 disrupts the polyA RNA exosome.

A) CDK13 IP-MS schema. B) Heatmap of average total peptides from anti-V5 IP-MS of CDK13 WT-V5 (n=3) or CLOVER-V5 (n=2). C) Log2 fold change CDK13^{WT}/control total peptides by (−) log p-value (two-tailed t test). Upper right quadrant indicates proteins with a (−) p-value <0.05 and a log fold change enrichment over control >3.3. D) Graphic depicting ZC3H14 phosphorylation sites identified from ZC3H14 IPed from either CDK13^{WT} - or CDK13^{mut}-expressing human melanoma cells. E) *In vitro* kinase assay of wild-type CDK13/CCNT1 using ZC3H14 full-length WT and S475A substrate. p= 0.00720098 2-tailed t-test

WT vs. S475A, n=3 each condition. F) Total peptides as a % of bait (ZC3H14 total peptides) for proteins with binding most regulated by CDK13 kinase activity. Mean +SD. n=biologic replicates. Gray dots = individual values. G) Box plot showing log2 fold change of siZFC3H1, ZC3H14^{S475A}, or ZC3H14^{S475E} as compared to the relevant control for ptRNAs (left), last exons (middle), or internal exons (right). Significantly changed genes (q<0.1) plotted for all RNA types in each experiment. Z1 = ZFC3H1, Z14 = ZC3H14. ptRNA = RNAs generated by usage of intronic polyadenylation sites. Internal exon = constitutive internal exon (non-alternatively spliced) isoform. In box plots, the black horizontal line indicates the median and whiskers extend to 1.5 × the interquartile range (IQR). Statistics in Table S5 (medians and two-sided Wilcoxom rank sum p values). H) IGV plot of *TP53* ptRNA which is regulated by CDK13, ZFC3H1, and ZC3H14 S475 phosphorylation. Scale = normalized RNA expression (note different scales). I) Doubling time of human melanoma cells expressing CDK13^{mut}, ZC3H14^{S475A}, ZC3H14^{S475E}, or CDK13^{mut}+ZC3H14^{S475A}. One-way ANOVA multiple comparisons.

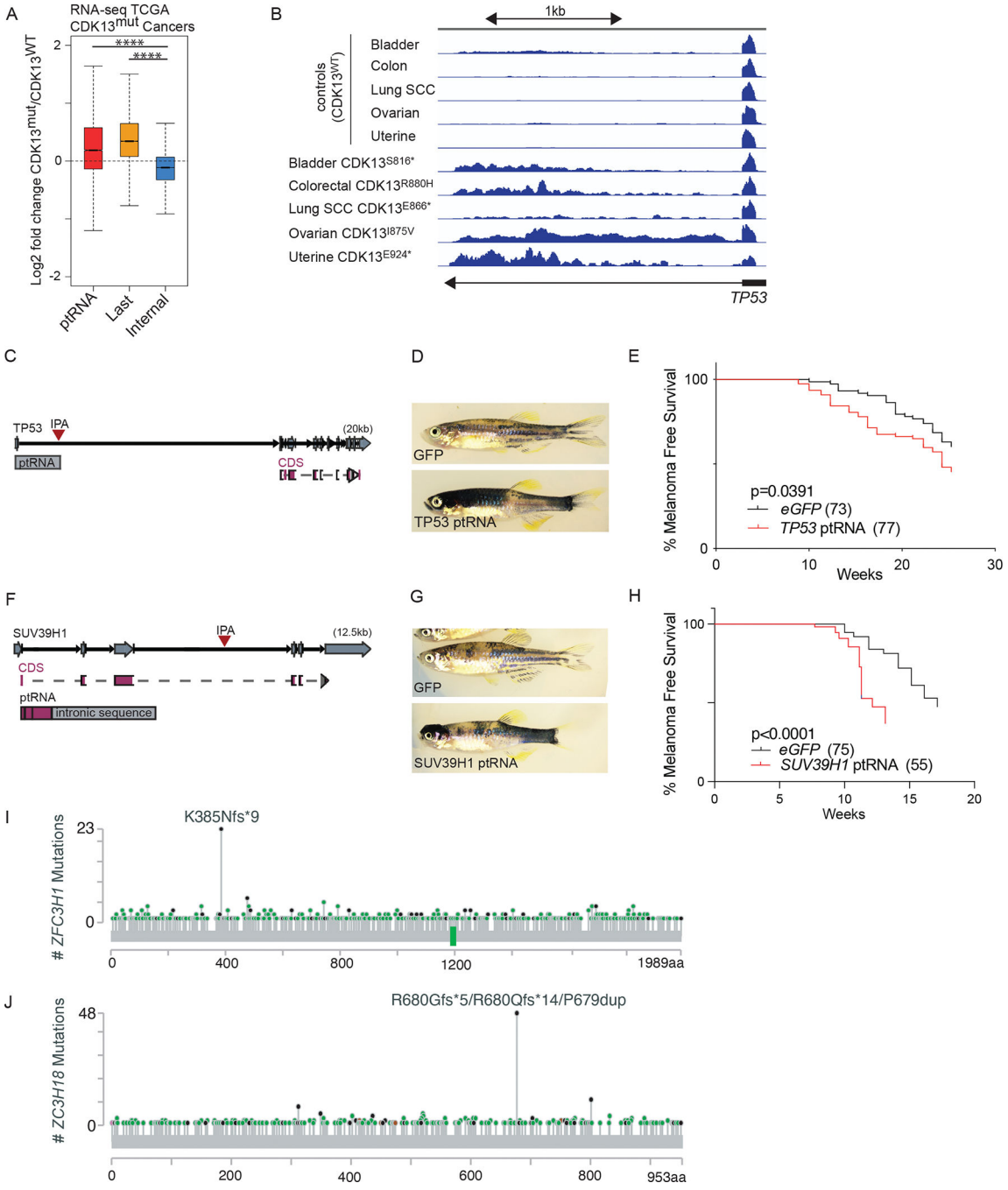

Figure 5: Prematurely Terminated RNA Accumulation is Oncogenic.

A) ptRNA quantification from somatic CDK13^{mut} (n=14) as compared to matched CDK13^{WT} (n=14) cancers (many types). ****=p<2.2e^{-16} (two-sided Wilcoxon rank sum) The black horizontal line indicates the median and whiskers extend to 1.5 × the interquartile range (IQR). B) IGV RNA-seq coverage plot of PAXT-target *TP53* ptRNA from sample subset from A). C) *TP53* ptRNA in *TP53* locus. IPA = intronic polyadenylation site. CDS = coding sequence. D-E) Triples melanoma model zebrafish with melanocyte-specific expression of EGFP vs. human *TP53* ptRNA. D) 7-week photos. E) % melanoma-free

survival (log-rank). (n)=zebrafish. F) *SUV39H1* ptRNA in *SUV39H1* locus. G-H) Triples melanoma model zebrafish with melanocyte-specific expression of EGFP vs. human *SUV39H1* ptRNA. G) 7-week photos. H) % melanoma-free survival (log-rank). I-J) Lollipop plots of *ZFC3H1* (I) and *ZC3H18* (J) mutations in non-redundant publicly available sequencing data from all cancers.

Table 1:

CDK13 Alterations Occur in All Genetic Subtypes in Melanoma TCGA Patients with DNA mutational and RNA expression data available.

	***CDK13* Mutated and Downregulated % (# mutated, # downregulated) (33/287 total)**	**All Other Cases % (n= cases) (254/287 total)**
BRAF V600 Mutations	36.4 (5, 7)	50.8 (129)
NRAS Q61 Mutations	36.4 (5, 7)	26.8 (68)
Other	27.3 (2, 7)	22.4 (57)

Table 2:

CDK13-Regulated PAXT Subunits Aie Mutated/Deleted in Melanoma TCGA Patients.

Gene	Mutation % (# of cases/287)
THOC2	7% (19)
ZFC3H1	5% (14)
ZC3H14	3% (8)
MTR4	2% (6)

Table 3:

CDK13 has a related but distinct biologic role and mechanism from CDK12.

	CDK13	**CDK12**
Mutated in Cancer	Melanoma (3.9%), cancer cell lines (8%)	Prostate (64, 65)
Mutated in Developmental Disorders	De novo heterozygous kinase domain mutations and truncating mutations cause developmental disorders that affect neural crest-derived tissues (congenital heart defects, dysmorphic facial features, and intellectual development disorder)(CHDFIDD)) (15–19)	Not detected
RNA Signature	No loss of DNA repair gene expression.	Loss of DNA repair gene expression (7, 8, 40, 66)
RNA Mechanism	Required to activate PAXT degradation of prematurely terminated RNAs.	Required to suppress usage of intronic polyadenylation sites (7) (8)